JACS
JOURNAL OF THE AMERICAN CHEMICAL SOCIETY
pubs.acs.org/JACS

Article

Supersaturation, Nucleation, and Phase Separation of Mesoscopic Systems

Jingyu Kang, Donghee Kim, Sanggeun Song, Jonghwa Han, Yongwon Jung, Sangwoon Yoon, Youngjae Ryu, Sungjee Kim, Byung Hyo Kim, Jeong-Mo Choi, Mino Yang, Joonkyung Jang, Taeghwan Hyeon, Jungwon Park,* Ji-Hyun Kim,* and Jaeyoung Sung*

Cite This: J. Am. Chem. Soc. 2025, 147, 46976−46985

Read Online

ACCESS | Metrics & More | Article Recommendations | Supporting Information

ABSTRACT: Supersaturation, nucleation, and phase separation are ubiquitous phenomena of great interest in both science and industry. However, a unified, quantitative understanding of these phenomena has yet to be achieved for mesoscopic systems. Here, we present a set of general equations that determine the monomer saturation degree, the size distribution, and the free energy of mesoscopic systems, as well as their phase-transition conditions. These equations reveal that, under supersaturation, the largest cluster size (LCS) is an important state variable; the supersaturation degree decreases with the LCS, approaching unity in the macroscopic limit. We identify the critical supersaturation, at which the nuclei undergo the phase transition to form large crystals. Below this critical supersaturation, the nucleus size distribution is either a unimodal function or a monotonically decreasing function of size, depending on the system and temperature. We also predict the most probable nucleus size and the direction of spontaneous changes of the LCS. Our theory provides a unified, quantitative explanation of the nucleus-size-distribution across six different systems, including nanoparticles and biological condensates. This work serves as a general theoretical framework useful for understanding and designing nucleation and phase transitions of mesoscopic systems.

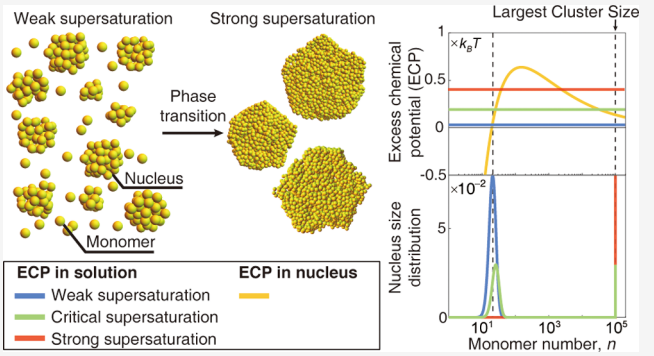

1. INTRODUCTION

Supersaturation and nucleation are universal thermodynamic phenomena observed across diverse systems, ranging from nanocrystals[1,2] and biological condensates[3,4] to fine dust and pollen,[5,6] raindrops,[7,8] clouds,[9−12] and even stars and galaxies.[13,14] These processes constitute the crucial, initial steps for all phase transitions, including crystallization. For development of nanocrystals, which have had significant impacts on materials science,[1,15,16] controlling nucleation and phase transition is particularly important and remains a central issue across various industrial fields. For example, precise control over the size and shape of quantum dots is essential for their optoelectronic and photovoltaic applications.[17] Additionally, it is critical to optimize the electrolyte interphase near electrodes for solid electrolyte batteries[18] and to achieve defect-free single-crystal silicon wafer formation and uniform thin-film deposition for semiconductor fabrication.[19] In recent years, the nucleation and phase separation of biomolecules in living cells, along with their biological implications, have also drawn a great deal of attention.[3,20−22]

Despite significant advances in these fields, our understanding of supersaturation, nucleation, and phase separation in mesoscopic material systems remains far from complete. The precise conditions under which mesoscopic crystals and biological condensates form from supersaturated solutions are still unknown. The thermodynamic origin of supersaturation and the equation governing the supersaturation degree have yet to be discovered. Moreover, it has long been elusive how the size distribution of nuclei depends on the chemical identity of monomers and solution environments, temperature, and total monomer concentration.

Since Gibbs and Thomson laid the foundation of nucleation theory in the late 19th century,[23] extensive varieties of models and theories have been developed to understand nucleation and phase transition phenomena.[24−30] According to the classical nucleation theory (CNT) based on the Gibbs−Thomson equation (GTE), nuclei smaller than a critical size should exhibit a monotonically decreasing size distribution and therefore cannot have a unimodal size distribution.[24,25,31] This

Received: June 27, 2025
Revised: November 21, 2025
Accepted: November 24, 2025
Published: December 3, 2025

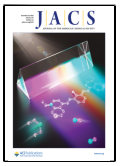

https://doi.org/10.1021/jacs.5c10868
J. Am. Chem. Soc. 2025, 147, 46976−46985

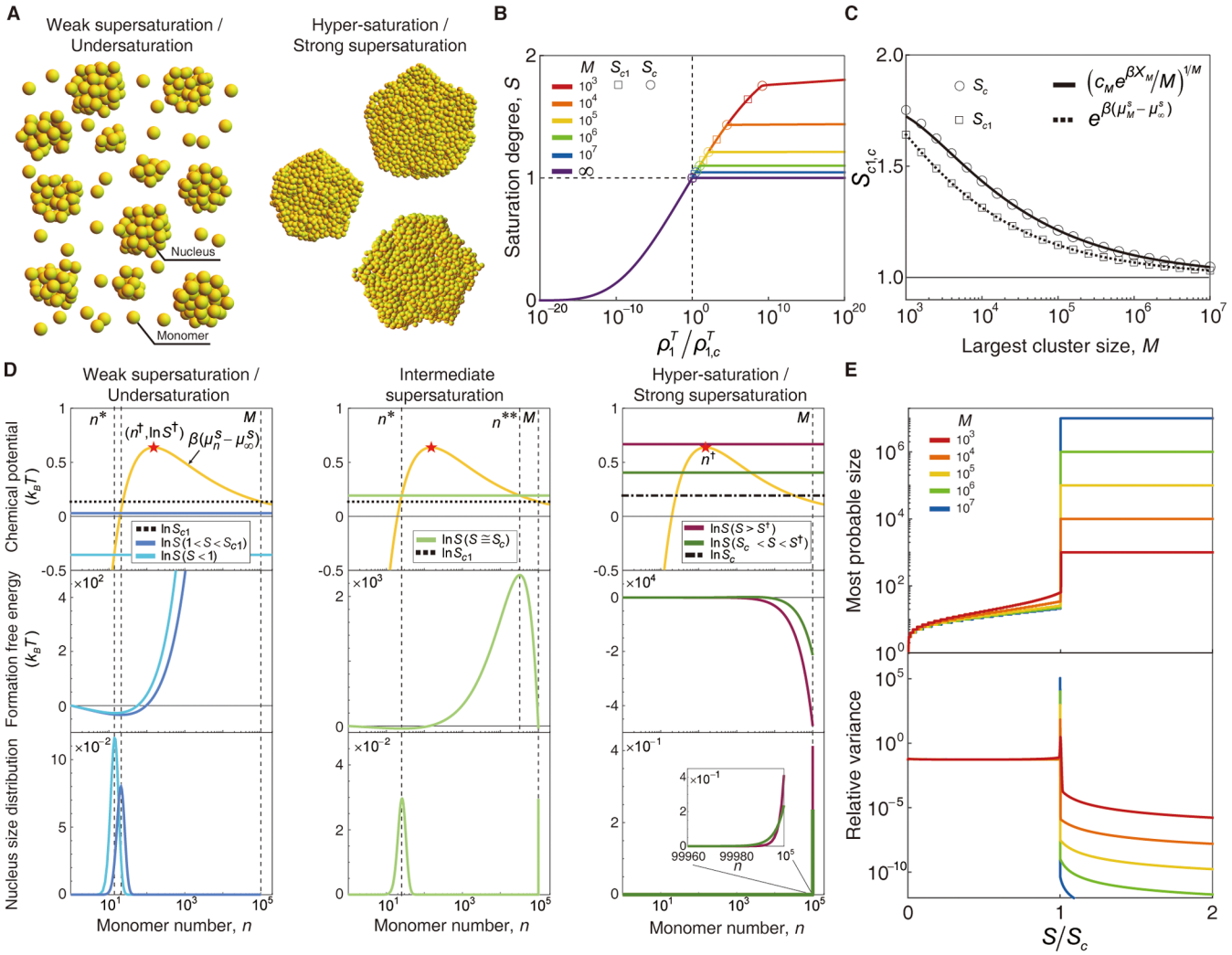

Figure 1. Equilibrium size distribution of nucleus seeds and large clusters. (A) Schematic representation of nucleus seeds and clusters at different total monomer concentration ρ_1^T and largest cluster size M. (left) Nucleus seeds dominant, undersaturation or weak supersaturation condition. (right) Large clusters dominant, strong supersaturation or hyper-saturation condition. (B) Relationship between the total monomer concentration, $\rho_1^T/\rho_{1,c}^T$ and saturation degree, S, obtained from eq 3a and 4 with the values of βc_1, βc_2, and c_3 given by 10, −50, and 4, respectively (Materials and Methods in Supporting Information). $\rho_{1,c}^T$ denotes the total monomer concentration when $S = 1$ (see text below eq 3a). (C) M dependence of S_{c1} and S_c. (squares) Critical supersaturation degree S_{c1} at which p_n undergoes the transition between a unimodal shape and a nonunimodal shape. (circles) Critical supersaturation degree S_c at which $p_{n^*} \cong p_M$. (solid line) eq 5a when $\rho_1^T/\rho_{1,c}^T = 1$. (dotted line) $\exp[\beta(\mu_M^s - \mu_\infty^s)]$. $\mu_n^s - \mu_\infty^s$ denotes the excess chemical potential (ECP) (eq 8). Both S_{c1} and S_c approach unity in the large-M limit. (D) n-dependence of ECP (top), free energy change associated with the formation of an n-mer from n monomers (center), and nucleus-size-distribution p_n (bottom) at various values of S. (yellow line) ECP. (star) The maximum value $\beta(\mu_{n^\dagger}^s - \mu_\infty^s)(\equiv \ln S^\dagger)$ of the thermal energy scaled ECP at $n = n^\dagger$ (Materials and Methods in Supporting Information). The horizontal lines represent the value of $\ln S$, or the thermal energy scaled excess chemical potential $\beta(\mu_1 - \mu_\infty^s)$ of monomers in solution, in (cyan) undersaturation ($S < 1$), (blue) weak supersaturation ($1 < S < S_{c1}$), (lime green) intermediate supersaturation ($S_{c1} < S \leq S_c$), (emerald green) strong supersaturation ($S_c < S < S^\dagger$), and (red) hyper-saturation ($S^\dagger < S$) conditions. The M value is set to be 10^5. When $S < S_{c1}$, the formation free energy has a local minimum at $n = n^*$, around which p_n has a unimodal peak. When $S_{c1} < S \leq S_c$, the formational free energy has a local maximum at $n = n^{**}$ ($>n^*$) as well as the local minimum at $n = n^*$. When $S \cong S_c$, the tail of p_n near $n = M$ becomes comparable to the peak around n^*. When $S_c < S < S^\dagger$, the tail of p_n dominates the peak around n^*. When $S^\dagger < S$, p_n monotonically increases with n. (inset) The divergent tails of p_n when $S_c < S < S^\dagger$ (emerald green line) and $S^\dagger < S$ (red line). (E) Dependence of the most probable size (upper) and the relative variance (lower) of nucleus size on S/S_c.

is also the case for modern generalizations of the CNT based on the density functional theories.[32−35] However, recent experimental studies have revealed the existence of mesoscopic nuclei with a unimodal size distribution across various systems, including electrolyte solutions,[36−39] semiconductor quantum dots,[40,41] noble metals,[42−47] biological condensates,[48,49] and amyloid protein fibrils.[50,51] There have been controversies over the origin of the monodisperse size distribution.[38,52,53]

Hill and Chamberlin (HC) developed a pioneering theory that predicts a unimodal size distribution for liquid droplets in equilibrium with undersaturated vapor by accounting for the translational and rotational motion of liquid droplets.[27] However, the HC theory invokes the unrealistic assumption that the liquid droplets have similar free energy as rigid bodies and its predicted droplet size distribution has not yet been experimentally verified. Recently, Sung and co-workers, and separately, Nelson and Friedman obtained similar unimodal

https://doi.org/10.1021/jacs.5c10868
J. Am. Chem. Soc. 2025, 147, 46976−46985

size distributions based on the molecular partition function formulation, applicable to gaseous systems, explaining the monodisperse size distribution of nanoparticles in condensed phases.[54−56] Nevertheless, these theories fail to explain a unimodal nucleus-size-distribution under supersaturation conditions.[57] More recently, applying a nonequilibrium density functional theory to diffusion-limited nucleation of macromolecules, Lutsko showed that nucleation proceeds by a two-step mechanism involving the formation of a metastable, solution droplet followed by ordering at its core.[32] Yet, no current theory defines the precise conditions under which mesoscopic nuclei undergo phase separation or provides equations that allow us to calculate the supersaturation degree and the size distribution of nuclei at a given temperature and total monomer concentration. A comprehensive theoretical framework that quantitatively explains supersaturation, nucleation, and phase separation across diverse mesoscopic systems remains to be established.

Here, addressing these issues, we present a set of equations that govern the size distribution and free energy of mesoscopic nuclei at a thermodynamic state defined by temperature, volume, total monomer concentration, and largest cluster size (LCS). For this purpose, we extended the molecular partition function formulation to encompass nuclei and clusters in condensed phases, explicitly accounting for microscopic interactions between nuclei and surrounding solvent molecules. Using this formulation, we present the equation governing the monomer saturation degree, which depends on the total monomer concentration, the nucleus free energy, temperature, and the largest cluster size (LCS). This equation reveals that supersaturation emerges even at equilibrium in a mesoscopic nuclei system with a finite LCS and its degree decreases with the LCS for a given total monomer concentration. We also present the explicit formula for the critical supersaturation degree at which phase separation occurs. Below this critical supersaturation, the equilibrium size distribution of nuclei is either a unimodal function or a monotonically decreasing function of size, depending on both the system and the surrounding environment, unless the LCS is constrained to remain below a critical size. Furthermore, we identify the conditions under which the LCS value spontaneously increases and predict the temperature and saturation degree dependencies of the most probable nucleus size.

Our analytic formula provides a unified, quantitative explanation of the nucleus-size-distribution obtained across six different experimental systems including nanoparticles and biological condensates. Most of these systems exhibit a unimodal size distribution under supersaturation conditions. Combined with modern computational science along with machine learning technique,[58−60] this work enables construction of physicochemical models with predictive capabilities for nucleation and phase transition of mesoscopic material systems.

2. RESULTS

We consider an ensemble of nuclei in a thermodynamic state defined by temperature T, system volume V, the total monomer number N_1^T, and the number, M, of monomers in the largest cluster within our system (Figure 1A). By applying Gibbs−Boltzmann's statistical thermodynamics to this ensemble, we obtain the three key equations for the equilibrium distribution of nucleus size, the free energy of the total nuclei system, and the monomer saturation degree.

2.1. Equilibrium Size Distribution. The equilibrium distribution of the number, n, of monomers in a nucleus, is obtained as (Materials and Methods in Supporting Information)

$$p_n = \frac{\exp(-\beta X_n)S^n}{\sum_{m=1}^{M}\exp(-\beta X_m)S^m} \tag{1}$$

where β denotes inverse thermal energy $(k_BT)^{-1}$ with k_B denoting the Boltzmann constant. X_n and S designate, respectively, the nonextensive free energy of a single n-mer, which is defined by $X_n \equiv f^s(n) - n\mu_\infty^s$ with $f^s(n)$ and μ_∞^s denoting the Helmholtz free energy of a single n-mer and the chemical potential of monomers in the macroscopic phase, and the saturation degree defined by $S = \rho_1/\rho_{sol}$, with ρ_1 and ρ_{sol} denoting the concentration of free monomers in solution and the solubility, i.e., the maximum concentration of free monomers in solution at equilibrium with a macroscopic phase. Note that p_n depends not only on the nonextensive free energy X_n, an intrinsic thermodynamic property of the nucleus system, but also on temperature T and saturation degree S, extrinsic variables that we can control. The equation governing saturation degree S and explicit analytic expression of X_n will be provided shortly.

2.2. Free Energy of Nucleation System. The Helmholtz free energy of the nucleation system determines the direction of spontaneous changes in the thermodynamic state of the system. For example, a spontaneous change in the value, M, of the LCS occurs in the direction in which the free energy decreases. An analytic expression of the Helmholtz free energy of the nucleation system is obtained as (Materials and Methods in Supporting Information)

$$A_M = N_1^T(\mu_\infty^s + k_BT[\ln S - \langle n\rangle_M^{-1}]) \tag{2}$$

where $\langle n\rangle_M$ denotes the mean nucleus size defined by $\langle n\rangle_M \equiv \sum_{n=1}^{M} np_n$. Equation 2 indicates that A_M/N_1^T linearly increases with $\mu_\infty^s + k_BT \ln S$, which is the chemical potential μ_1 of monomers in solution. To calculate p_n and A_M using eqs 1 and 2, we need to calculate saturation degree S.

2.3. Saturation Degree. Saturation degree S is dependent on the total monomer concentration ρ_1^T as well as temperature and the nonextensive free energy, X_n, of an n-mer. The equation governing saturation degree S is obtained as (Materials and Methods in Supporting Information):

$$\sum_{n=1}^{M}\xi_n S^n = \rho_1^T/\rho_{1,c}^T \tag{3a}$$

$$\xi_n \equiv \frac{n\exp(-\beta X_n)}{\sum_{m=1}^{M} m\exp(-\beta X_m)} \tag{3b}$$

where $\rho_{1,c}^T$ is defined as $\rho_{1,c}^T \equiv V^{-1}\sum_{n=1}^{M} n\exp(-\beta X_n)$. Since $\sum_{n=1}^{M}\xi_n = 1$, eq 3a yields $S = 1$ when $\rho_1^T = \rho_{1,c}^T$. The value of S is greater (smaller) than unity when ρ_1^T is greater (smaller) than $\rho_{1,c}^T$. One can solve eq 3a numerically to determine saturation degree S as a function of temperature and the total monomer concentration for any nuclei systems, provided that X_n can be computed. An approximate analytic solution of eq 3a and the dependence of saturation degree on the total monomer concentration and the largest cluster size are discussed in Discussion.

https://doi.org/10.1021/jacs.5c10868
J. Am. Chem. Soc. 2025, 147, 46976−46985

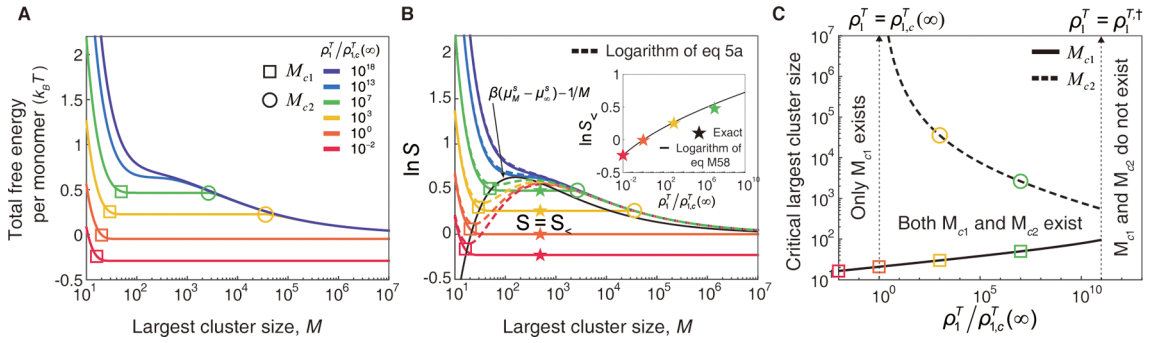

Figure 2. Largest cluster size dependence of Helmholtz free energy, saturation degree, and size distribution. (A) (colored solid lines) M dependence of the Helmholtz free energy A_M of the total system divided by the total monomer number N_T at various $\rho_1^T/\rho_{1,c}^T(\infty)$ values with $\rho_{1,c}^T(\infty)(\equiv V^{-1}\sum_{n=1}^{\infty} n e^{-\beta X_n})$. The y axis represents the value of $A_M/N_T - \mu_\infty^s$ in unit of thermal energy. (B) M dependence of ln$S$ (colored solid lines), the logarithm of eq 5a (colored dashed lines), and $\beta(\mu_M^s - \mu_\infty^s) - 1/M$ with values of βc_1, βc_2, and c_3 identical to those used in Figure 1 (black solid line). In (A) and (B), the square and circles symbols represent values of two roots, M_{c1} and M_{c2}, of $S(M) = S_<$ at given values of $\rho_1^T/\rho_{1,c}^T(\infty)$, respectively. A_M decrease with M for the M values less than M_{c1} or greater than M_{c2}, where eq 5a provides a good approximation of $S(M)$. A_M is nearly independent of M for the M values between M_{c1} and M_{c2}, where the M-independent S is designated by $S_<$. (inset) Dependence of ln$S_<$ on $\rho_1^T/\rho_{1,c}^T(\infty)$: Exact results (symbols) and logarithm of eq M58 in Materials and Methods in Supporting Information (line). (C) ρ_1^T dependence of M_{c1} and M_{c2} (solid and dashed lines). When $\rho_1^T < \rho_{1,c}^T(\infty)$, only M_{c1} exists; when $\rho_1^T > \rho_1^{T\dagger}$, neither M_{c1} nor M_{c2} exists; but when $\rho_{1,c}^T(\infty) < \rho_1^T < \rho_1^{T\dagger}$, both critical sizes exist.

We note here that, in the infinite-M limit, the value of S satisfying eq 3a cannot be greater than unity for any finite ρ_1^T. For this reason, supersaturation is negligible in solution at equilibrium with a macroscopic system. However, in solution at equilibrium with mesoscopic nuclei systems with finite M values, supersaturation ($S > 1$) can emerge when ρ_1^T is greater than $\rho_{1,c}^T$.

Equations 1−3 constitute the complete set of thermodynamic equations that govern the size distribution, total free energy, and saturation degree of a general mesoscopic system. To use them in practical applications, however, we need an explicit expression of the nonextensive free energy, X_n, which varies depending on a system of interest.[61]

2.4. Nucleus Model & Free Energy. We introduce a microscopic model of a nucleus in solution. In this model, we account for not only the translational, rotational, vibrational motion of a nucleus but also its microscopic interaction with the surrounding molecules and solvents, often overlooked in nucleation theories. The electronic energy contributions from the edge, surface, and core of the nucleus to its total free energy are also taken into account (Materials and Methods in Supporting Information).

To calculate thermodynamic properties of an ensemble of nuclei in solution, we develop the solution-phase molecular partition function formalism (Materials and Methods in Supporting Information). This solution-phase molecular partition function formalism enables us to obtain analytic expressions of the chemical potential and free energy of a single nucleus in terms of temperature and the microscopic properties of the nucleus, such as the nucleus size, the vibrational frequency distribution, the energy difference between the core part and the surface part, and the interaction potential between the nucleus and surrounding molecules.

The free energy $f^s(n)$ of an n-mer consists of an extensive part, $n\mu_\infty^s$, which grows linearly with system size, and a remaining nonextensive part, X_n.[61] Our nucleus model yields explicit expressions for both parts (Materials and Methods in Supporting Information). The extensive part is dominantly contributed by the vibrational and electronic degrees of freedom of a nucleus and the exclusion of solvent molecules by the nucleus. The chemical potential μ_∞^s of monomers in a macroscopic phase determines saturation level ρ_{sol} of monomers in solution at equilibrium with the macroscopic phase (Materials and Methods in Supporting Information).

For our nucleus model, the nonextensive part X_n of the free energy of a nucleus can be cast into the following form,

$$X_n = c_1 n^{2/3} + c_2 n^{1/3} - k_B T c_3 \ln n + \text{constant in } n \qquad (4)$$

where the analytic expressions of c_1, c_2, and c_3 are given in Materials and Methods in Supporting Information. These coefficients are only weakly dependent on temperature and size n for a quasi-spherical nucleus. The first two terms on the right-hand-side (r.h.s.) of eq 4 originate from the energy difference between the surfaces and the core of the nucleus as well as microscopic interactions between nucleus and surrounding molecules. The third term originates from translational and rotational motion and the configurational degeneracy of the nucleus. We note that, for a large spherical nucleus, eq 4 shares the same mathematical form as Dillmann and Meier (DM)'s phenomenological free energy expression.[26]

Equation 4 has a finite application range. For the cluster of Lennard-Jones (LJ) particles with the Mackay icosahedral geometry,[62] we find eq 4 applicable to clusters containing more than 13 particles (Figure S1). The minimum nucleus size to which eq 4 is applicable depends on the system of interest. However, even when we are interested in the size distribution of tiny nuclei to which eq 4 does not hold, we can still obtain the size distribution from eqs 1 and 3a, using accurate X_n of the nuclei. In principle, it is possible to calculate X_n of small nuclei by combining the first-principle molecular dynamics simulation and our solution-phase molecular partition function formulation.[63−66]

3. DISCUSSION

Saturation degree S exhibits two distinct phases in its dependence on the total monomer concentration and LCS. When saturation degree is below a critical supersaturation, it is sensitive to the total monomer concentration but largely independent of the LCS. Conversely, when the saturation degree is above the critical supersaturation, it is sensitive to the

https://doi.org/10.1021/jacs.5c10868
J. Am. Chem. Soc. 2025, 147, 46976−46985

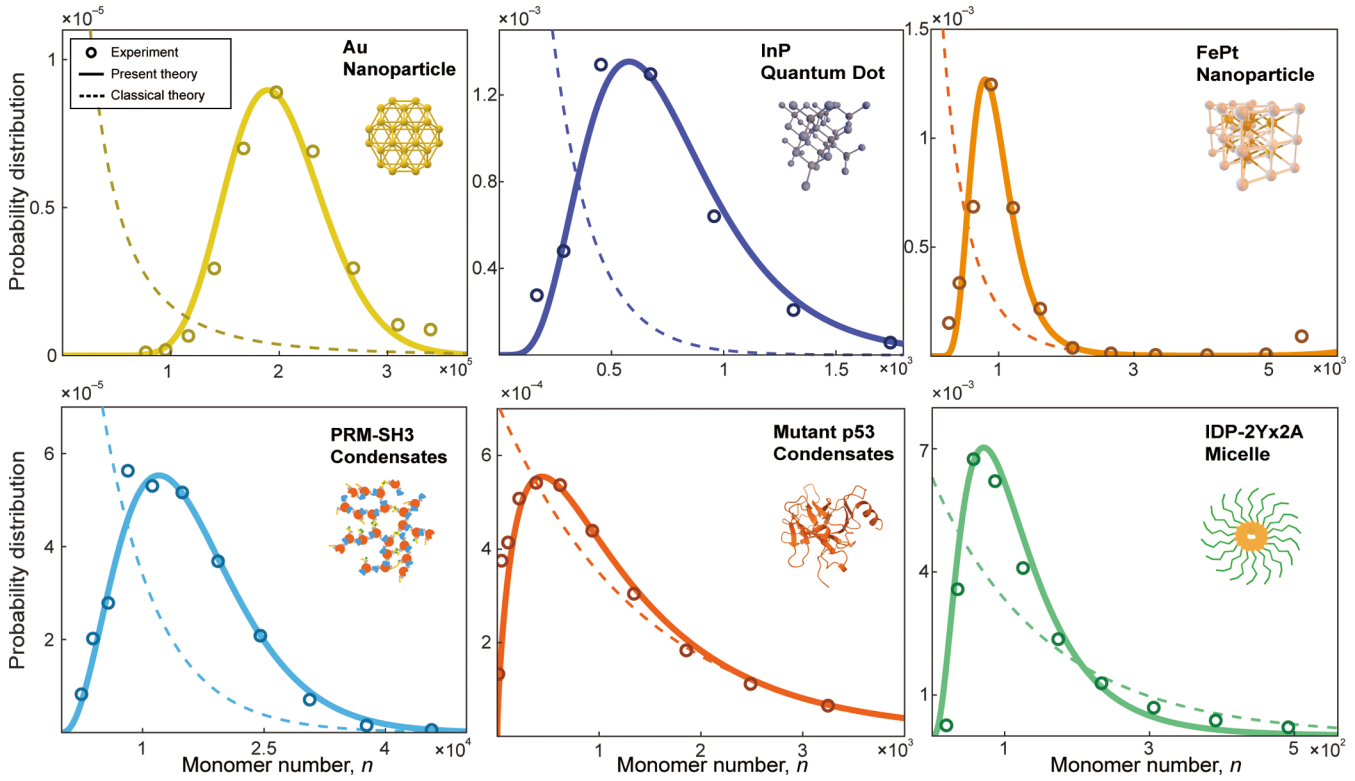

Figure 3. Nucleus-size-distributions of various nucleation systems. 1st row: Nucleus-size-distributions of Au nanoparticles (left), InP quantum dots (middle), and FePt nanoparticles (right) (see Figure S7 for their TEM images). 2nd row: Nucleus-size-distributions of metal ion-mediated PRM-SH3 condensates[70] (left), mutant p53 tumor suppressor protein condensates[71] (middle) and biosurfactant micelles[72] (right). The biosurfactant micelles are composed of an amphiphilic biopolymer derived from a hydrophilic intrinsically disordered protein (IDP) sequence fused with a genetically encoded hydrophobic domain. (symbols) Experimental data. (solid lines) Results of eqs 1 and 4. The optimized values of adjustable parameters are presented in Table 1. (dotted lines) Results of the classical nucleation theory based on GTE. They are calculated by eqs 1 and 4 with $c_2 = c_3 = 0$.

LCS but largely independent of the total monomer concentration.

To show this, let us first consider the case where S is so small that $\xi_n S^n$ rapidly decreases with n. In this case, eq 3a can be approximated by $\sum_{n=1}^{\infty} \xi_n S^n = \rho_1^T/\rho_{1,c}^T$, whose solution, saturation degree S, is essentially independent of M. A necessary condition for this case is that the series $\{\xi_n S^n\}$ has a tail that decreases with n, that is, $\partial_n(\xi_n S^n)|_{n=M} = \partial_n \exp(\ln n - \beta X_n + n \ln S)|_{n=M} < 0$ or $\ln S < \beta(\mu_M^s - \mu_\infty^s) - M^{-1}$. In the latter equation, $\mu_M^s - \mu_\infty^s$ denotes the excess chemical potential (ECP) defined by $\partial_M X_M[\equiv \partial_M(f^s(M) - M\mu_\infty^s)]$ (Figure S2A,B). Saturation degree S with a negligible M dependence will be designated by $S_<$, which is a function of $\rho_1^T/\rho_{1,c}^T$ and $\{\beta X_n\}$ only (Figure 1B). An approximate analytic expression $S_<^{(a)}$ of $S_<$ is provided in eq M58 (see Materials and Methods in Supporting Information).

In the other case where $\ln S$ is significantly greater than $\beta(\mu_M^s - \mu_\infty^s) - M^{-1}$, the series $\{\xi_n S^n\}$ in eq 3a has a divergent tail. When $\xi_n S^n$ has a divergent tail, the value of S is sensitive to the largest cluster size, M (Figures S2A,B), which will be designated by $S(M)$. We obtain a simple, approximate expression of $S(M)$ from eq 3a using the maximum term method as

$$S(M) \cong S_c(M)(\rho_1^T/\rho_{1,c}^T)^{1/M}[\equiv S_a(M)],\ (\rho_1^T \gg \rho_{1,c}^T) \tag{5a}$$

$$S_c(M) = \exp\{M^{-1}(\beta X'_M - \ln M + \ln c_M)\} \tag{5b}$$

where $S_c(M)$ denotes the critical supersaturation dependent on M. In eq 5b, c_M is defined by $c_M = \sum_{n=1}^{M} n e^{-\beta X'_n}$ with X'_n denoting the n-dependent part of X_n (Materials and Methods in Supporting Information). The value of c_M quickly approaches a constant, c_∞, as M increases. Both $S(M)$ and $S_c(M)$ monotonically decrease with M. The approximate results calculated from eq 5a are in excellent agreement with the exact numerical solutions, $S(M)$, of eq 3a. (Figure 2B). Equation 5a tells us that $S(M)$ is almost the same as $S_c(M)$ while the value of $\rho_1^T/\rho_{1,c}^T(\gg 1)$ increases by several orders of magnitude for a typical M value, which is greater than 10^3 in most experiments. This results in the saturation degree being effectively bound (Figure 1B). Note that both $S(M)$and $S_c(M)$ approach unity in the large-M limit (Figure 1C), which indicates that supersaturation disappears in solution at equilibrium with a macroscopic phase.

The shape of the nucleus-size-distribution predicted by eqs 1 and 4 exhibits the phase transition when saturation degree S passes through the critical supersaturation S_c given in eq 5b. The nucleus-size-distribution has a divergent tail when $S > S_c$. In this case, the most probable size is the largest cluster size M regardless of the detailed form of X_n. In contrast, when $S < S_c$, the nucleus-size-distribution is either a monotonically decreasing function or a unimodal function of nucleus size, depending on the nonextensive free energy X_n, with the most probable size far smaller than M.

To show this, let us consider the logarithmic derivative of eq 1,

https://doi.org/10.1021/jacs.5c10868
J. Am. Chem. Soc. 2025, 147, 46976−46985

Table 1. Optimized Values of Parameters Extracted from the Nucleus Size Distribution for Various Nucleation Systems[a]

parameter	σ_s (nm)	βc_1	βc_2	c_3	ln$S$
Au nanoparticle	0.159	1.05×10^{-2}	−1.56	6.05	-6.77×10^{-5}
InP quantum dot	0.229	4.76×10^{-1}	−4.18	4.00	1.11×10^{-2}
FePt nanoparticle	0.188	1.45	−15.5	4.00	3.92×10^{-2}
PRM-SH3 condensate	3.27	3.85×10^{-6}	−0.230	1.71	-2.88×10^{-4}
mutant p53 condensate	4.40	8.11×10^{-2}	−0.900	0.200	1.46×10^{-3}
IDP-2Yx2A micelle	3.00	7.93×10^{-1}	−3.14	2.24	3.51×10^{-2}

[a]The values of parameters extracted from our analysis of the distribution, $P(r)$, of the nucleus's radius are presented for six different experimental systems. Here, $P(r)$ is related to p_n by $P(r) \propto p_n(\mathrm{d}n/\mathrm{d}r) = (3r^2/\sigma_s^3)p_{n=(r/\sigma_s)^3}$, where p_n is given by eqs 1 and 4. σ_s denotes the characteristic length scale defined by $n = (r/\sigma_s)^3$ (see Supplementary Text 4 in Supporting Information for details on the method used to determine σ_s values). Figure 3 presents the results of our analyses for p_n across these experimental systems. c_1, c_2, and c_3 are parameters characterizing the non-extensive free energy, X_n, given by eq 4. β denotes $(k_BT)^{-1}$ with k_B being the Boltzmann constant. The extracted parameter values obtained for these nucleation systems satisfy the condition under which the excess chemical potential, $\mu_n^s - \mu_\infty^s$, of monomers in a nucleus has a non-monotonic size dependence, i.e., $c_f < 2c_e + 3k_BTc_m$ (see eq 8), or equivalently $\frac{2}{3}\beta c_1 < -\frac{2}{3}\beta c_2 + 3c_3$. Note that PRM-SH3 condensates, mutant p53 condensates, and IDP-2Yx2A micelles can be regarded as liquid-like droplets, different from nanoparticles or quantum dots; in this case, the value of c_3 can be lower than four.[26] For most of the nucleation systems investigated, the value of saturation degree S is less than or equal to that of the first critical supersaturation level, S_{c1}, defined by $S_{c1} = \exp[\beta(\mu_M^s - \mu_\infty^s)]$ with M denoting the largest cluster size, estimated as $M = (r_{max}/\sigma_s)^3$, where r_{max} is the largest nucleus radius observed in the experimental data. The value of lnS_{c1} calculated from the definition is as follows: -2.59×10^{-5} for Au nanoparticles, 1.44×10^{-2} for InP quantum dots, 3.76×10^{-2} for FePt nanoparticles, -2.18×10^{-6} for PRM-SH3 condensates, 1.76×10^{-3} for mutant p53 condensates, and 3.51×10^{-2} for IDP-2Yx2A micelles. By contrast, for FePt nanoparticles, the value of S is greater than that of S_{c1}, indicating the presence of a tail that increases with size near the largest size as shown in Figure 3

$$\partial_n \ln p_n = \ln S - \beta(\mu_n^s - \mu_\infty^s) \tag{6}$$

p_n has a local maximum at $n = n^*$ if there exists n^* satisfying

$$\ln S = \beta(\mu_{n^*}^s - \mu_\infty^s) \text{ and } \partial_n \mu_n^s|_{n=n^*} > 0 \tag{7a}$$

On the other hand, p_n has a local minimum at $n = n^{**}$ if there exists n^{**} satisfying

$$\ln S = \beta(\mu_{n^{**}}^s - \mu_\infty^s) \text{ and } \partial_n \mu_n^s|_{n=n^{**}} < 0 \tag{7b}$$

According to the GTE, μ_n^s is a monotonically decreasing function of n. Consequently, the equilibrium nucleus-size-distribution obtained based on the GTE cannot have a unimodal size distribution with the maximum at $n = n^*$, at which μ_n^s should have a positive slope as defined in eq 7a.

For our nucleus model, however, the ECP of a nucleus can be either a monotonically decreasing function or a non-monotonic function of n. The analytic expression of the ECP can be obtained from eq 4 as

$$\mu_n^s - \mu_\infty^s \cong \frac{c_f}{n^{1/3}} - \frac{c_e}{n^{2/3}} - k_BT\frac{c_m}{n} \tag{8}$$

with $c_f = (2/3)c_1$, $c_e = -(1/3)c_2$, and $c_m = c_3$. c_f and c_m assume positive values, while c_e can be negative or positive (Materials and Methods in Supporting Information). The ECP given in eq 8 monotonically decreases with n for the entire range of n when $c_1 + c_2 > (9/2)k_BTc_3$, but is a nonmonotonic function of n with a single peak when $c_1 + c_2 < (9/2)k_BTc_3$, as shown in Figure 1D (Supplementary Text 1 in Supporting Information).

In case where the ECP given in eq 8 monotonically decreases with n for the entire range of n, p_n has two qualitatively different shapes depending on saturation degree. p_n is a monotonically decreasing function of n, i.e., $\partial_n \ln p_n = \ln S - \beta(\mu_n^s - \mu_\infty^s) < 0$, when $\ln S < \beta(\mu_M^s - \mu_\infty^s)(\equiv \ln S_{c1})$. On the other hand, when $S > S_{c1}$, p_n becomes a convex function of n with a single minimum at $n = n^{**}$. As saturation degree further surpasses the critical supersaturation $S_c(>S_{c1})$, p_n becomes the convex function with a divergent tail (Figure S3). An example for this case is a system of clusters of Lennard-Jones particles with Mackay icosahedral geometry at low temperatures (Figure S1).[62,67] In the infinite M limit, this size-dependency of p_n is qualitatively the same as the J. Frenkel's nucleus-size-distribution based on the CNT[25] (Figure S4).

In case where the ECP is a nonmonotonic function of size n, p_n given in eq 1 assumes three qualitatively different shapes depending on saturation degree. When $S < S_{c1}(\equiv \exp[\beta(\mu_M^s - \mu_\infty^s)])$, n^* defined in eq 7a exists but n^{**} defined in eq 7b does not; consequently, p_n is a unimodal function of n with a single peak at nucleus size n^* (see Figure 1D). This is the case for most systems of colloidal nanoparticles at room temperatures and other nucleation systems with monodisperse size distributions (Figure 3 and Table 1). On the other hand, when $S > S_{c1}$, p_n has both the peak at $n = n^*$ and the local minimum at $n = n^{**}$. As S surpasses S_c given in eq 5b, p_n acquires a quasi-exponential, divergent tail at large n values near M, which dominates the peak at n^*. During this transition (Figure 1B), the most probable nucleus size undergoes a sudden jump from n^* to M and the relative variance of the nucleus size reaches its maximum, unless M is constrained to remain below the critical size $n^\dagger[\equiv(c_e/c_f + \sqrt{(c_e/c_f)^2 + 3k_BTc_m/c_f})^3]$ at which the ECP given in eq 8 assumes its maximum (Figures 1e and S5). This transition signifies the phase transition from nucleus seeds to large crystals (Figure 1). Finally, under the hyper-saturation conditions satisfying $\ln S > \beta(\mu_{n^\dagger}^s - \mu_\infty^s)$, p_n monotonically increases with n (the right panel of Figure 1D), because $\partial_n \ln p_n = \ln S - \beta(\mu_n^s - \mu_\infty^s) > 0$ for all n according to eq 6 (Figure 1B).

The unimodal size distribution p_n, which emerges when $S < S_c$, can be approximated by Gaussian around the most probable nucleus size, i.e., $p_n \cong p_{n^*}e^{-(n-n^*)^2/2\sigma_n^2}$ where σ_n^2 is given by $(\partial_n \beta\mu_n^s|_{n=n^*})^{-1}$. The most probable size n^* can be obtained by solving eqs 7a and 8; when S is close to unity, n^* can be approximated by (Materials and Methods in Supporting Information):

https://doi.org/10.1021/jacs.5c10868
J. Am. Chem. Soc. 2025, 147, 46976−46985

$$n^* \approx n_0\left(1 + \frac{3n_0 \ln S}{c_m + c_f n_0^{2/3}/k_B T}\right), (n^* < n^\dagger) \quad (9)$$

where n_0 denotes the most probable nucleus size when $S = 1$, defined by $n_0 \equiv 8^{-1}[c_e/c_f + \sqrt{(c_e/c_f)^2 + 4k_B T c_m/c_f}]^3$. Equation 9 shows that n^* increases with both temperature and saturation degree. Note that n^* cannot be greater than $n^\dagger$. This is because μ_n^s decreases with n for n greater than $n^\dagger$ while n^* should satisfy $\partial_n \mu_n^s|_{n=n^*} > 0$ by definition (see eq 7a).

In most experiments, the LCS, M, is not controlled, with only a few exceptions.[68,69] Then, a spontaneous change in M values occurs in the direction in which the Helmholtz free energy, A_M, of the total system decreases. According to eq 2, M dependence ofA_M is determined by $\ln S - \langle n\rangle_M^{-1}$, but $\langle n\rangle_M^{-1}$ is negligible compared to $\ln S$ in most cases. For this reason, A_M has qualitatively the same M-dependence as $\ln S$ (Figures 2A, B). When S is given by $S(M)$, which is the decreasing function of M, A_M decreases with M as well. However, when S is given by $S = S_<$, essentially independent of M, A_M has negligible M dependence.

A_M exhibits distinct M-dependence, depending on total monomer concentration ρ_1^T (Supplementary Text 2 in Supporting Information). In case where ρ_1^T is higher than threshold value $\rho_1^{T\dagger}$, saturation degree S and hence A_M decrease with M for the entire M values (Figure 2), which is unusual. Under the usual supersaturation conditions satisfying $\rho_{1,c}^T(\infty)(\equiv V^{-1}\sum_{n=1}^{\infty} n e^{-\beta X_n}) < \rho_1^T < \rho_1^{T\dagger}$, the M value spontaneously increases only up to M_{c1} but it does not have a preferred direction of change while the M value is within interval $M_{c1} < M < M_{c2}$ where M_{c1} and M_{c2} denotes the two roots of $S(M) = S_<$ (squares and circles in Figure 2A,B). Only after the M value reaches M_{c2} by unbiased random fluctuations, M values can spontaneously increase up to infinity and the macroscopic phase transition occurs. In undersaturation conditions with ρ_1^T being even lower than $\rho_{1,c}^T(\infty)$, M_{c2} does not exist and the M value spontaneously increases only up to M_{c1}; therefore, a macroscopic phase transition does not occur.

Equations 1 and 4 provide a quantitative explanation of the nucleus-size-distribution across various experimental systems, including not only gold, InP, and FePt nanoparticles but also biological condensates such as PRM-SH3 condensates,[70] p53 condensates,[71] and micelles[72] (Figure 3). This agreement between theory and experiment indicates that the nonextensive free energy X_n assumes the similar analytic form to eq 4 for both nanoparticles and biological condensates, although the values of the coefficients appearing in eq 4 differ from system to system. We note here that, for micelles and biological condensates, the monomer number is also referred to as aggregation number.

From the quantitative analysis, we extract the three parameters characterizing the nonextensive free energy X_n and saturation degree S for all experimental systems investigated. For most systems, p_n exhibits a unimodal shape, for which the ECP extracted from our quantitative analysis has the nonmonotonic dependence on n and the extracted value of S is not greater than S_{c1} in accordance with our theory (Table 1). However, for the data obtained from the FePt nanoparticle system, p_n has a small tail that increases with n. As discussed before, this kind of tail emerges when the ECP has the nonmonotonic size dependence and S exceeds S_{c1}.

We emphasize that eqs 1−3a of the present theory are applicable to a system of nuclei regardless of their sizes, given that accurate expression of their X_n is available. On the other hand, the expression for X_n given in eq 4 has a finite application range as described below eq 4. To address anonymous reviewer's comment, we note here that the application range of the present theory is not limited to mesoscopic systems with finite values of the LCS. In the infinite LCS limit, this theory describes saturation, nucleation, and phase transition of a macroscopic system.

A comparison between our theory with the previous nucleation theories is presented in Supplementary Text 3 in Supporting Information, for lack of space.

4. CONCLUSIONS

The size-distribution, free energy, and saturation degree S of mesoscopic nuclei systems obey eqs 1−3a. Supersaturation emerges in solution even at equilibrium with mesoscopic nuclei with a finite LCS and their phase transition occurs when saturation degree surpasses the critical supersaturation S_c given in eq 5a. When $S < S_c$, p_n is either a unimodal function or a monotonically decreasing function of size n, depending on the size-dependence of the nonextensive free energy X_n. An accurate expression of X_n, eq 4, is obtained for a microscopic model of nucleus in solution, according to which the chemical potential in a small nucleus can strongly deviate from the Gibbs−Thomson equation. Equation 1 and 4 provide a unified, quantitative explanation of the nucleus-size-distribution across nanoparticles and biological condensates. It is predicted that the most probable size of nanoparticles increases with temperature and the total monomer concentration but only up to a critical size $n^\dagger$. The LCS value, M, spontaneously increases when $M < M_{c1}$ or $M > M_{c2}$, but it does not have a preferred direction of spontaneous change when $M_{c1} < M < M_{c2}$ under usual supersaturation conditions. The present theory is applicable to diverse nucleation and phase separation phenomena occurring in nature and industry.[73−79]

■ ASSOCIATED CONTENT

Data Availability Statement

All data and codes are available from the corresponding authors upon request.

Supporting Information

The Supporting Information is available free of charge at https://pubs.acs.org/doi/10.1021/jacs.5c10868.

Materials and methods, additional experimental details, derivation of equations, size dependence of excess chemical potential, comparison with the previous nucleation theories, temperature-dependent shape transition, largest cluster size (M) dependence, saturation degree dependent size distribution, comparison between equilibrium size distributions, and ex-situ experiment of nanoparticle (PDF)

■ AUTHOR INFORMATION

Corresponding Authors

Jungwon Park − *Center for Nanoparticle Research, Institute for Basic Science (IBS), Seoul 08826, Korea; School of Chemical and Biological Engineering, Institute of Chemical Process Seoul National University, Seoul 08826, Korea; Institute of Engineering Research, College of Engineering, Seoul National University, Seoul 08826, Korea; Advanced*

https://doi.org/10.1021/jacs.5c10868
J. Am. Chem. Soc. 2025, 147, 46976−46985

Institute of Convergence Technology, Seoul National University, Suwon, Gyeonggi 16229, Korea; orcid.org/0000-0003-2927-4331; Email: jungwonpark@snu.ac.kr

Ji-Hyun Kim − *Global Science Research Center for Systems Chemistry, Creative Research Initiative Center for Chemical Dynamics in Living Cells, and Department of Chemistry, Chung-Ang University, Seoul 06974, Korea;* orcid.org/0000-0003-1535-7224; Email: jihyunkim@cau.ac.kr

Jaeyoung Sung − *Global Science Research Center for Systems Chemistry, Creative Research Initiative Center for Chemical Dynamics in Living Cells, and Department of Chemistry, Chung-Ang University, Seoul 06974, Korea;* orcid.org/0000-0003-0712-296X; Email: jaeyoung@cau.ac.kr

Authors

Jingyu Kang − *Global Science Research Center for Systems Chemistry, Creative Research Initiative Center for Chemical Dynamics in Living Cells, and Department of Chemistry, Chung-Ang University, Seoul 06974, Korea;* orcid.org/0000-0002-7037-4433

Donghee Kim − *Global Science Research Center for Systems Chemistry, Creative Research Initiative Center for Chemical Dynamics in Living Cells, and Department of Chemistry, Chung-Ang University, Seoul 06974, Korea;* orcid.org/0009-0002-5421-4189

Sanggeun Song − *Department of Chemical and Biomolecular Engineering, University of California, Berkeley, Berkeley, California 94720, United States; Chemical Sciences Division, Lawrence Berkeley National Laboratory, Berkeley, California 94720, United States;* orcid.org/0000-0002-5827-3496

Jonghwa Han − *Global Science Research Center for Systems Chemistry, Creative Research Initiative Center for Chemical Dynamics in Living Cells, and Department of Chemistry, Chung-Ang University, Seoul 06974, Korea;* orcid.org/0009-0002-9213-7268

Yongwon Jung − *Global Science Research Center for Systems Chemistry, Chung-Ang University, Seoul 06974, Korea; Department of Chemistry, Korea Advanced Institute of Science and Technology, Daejeon 34141, Korea;* orcid.org/0000-0002-1034-9797

Sangwoon Yoon − *Department of Chemistry, Chung-Ang University, Seoul 06974, Korea;* orcid.org/0000-0001-5705-4569

Youngjae Ryu − *Department of Chemistry, Pohang University of Science and Technology, Pohang 37673, Korea;* orcid.org/0009-0006-2363-5131

Sungjee Kim − *Department of Chemistry, Pohang University of Science and Technology, Pohang 37673, Korea;* orcid.org/0000-0002-1289-1926

Byung Hyo Kim − *Center for Nanoparticle Research, Institute for Basic Science (IBS), Seoul 08826, Korea; School of Chemical and Biological Engineering, Institute of Chemical Process Seoul National University, Seoul 08826, Korea; Department of Materials Science and Engineering, Soongsil University, Seoul 06978, Korea;* orcid.org/0000-0002-4098-0053

Jeong-Mo Choi − *Global Science Research Center for Systems Chemistry, Chung-Ang University, Seoul 06974, Korea; Department of Chemistry and Chemistry Institute for Functional Materials, Pusan National University, Busan 46241, Korea*

Mino Yang − *Department of Chemistry, Chungbuk National University, Cheongju, Chungbuk 28644, Korea;* orcid.org/0000-0001-9504-0280

Joonkyung Jang − *Department of Nanoenergy Engineering, Pusan National University, Busan 46241, Korea;* orcid.org/0000-0001-9028-0605

Taeghwan Hyeon − *Center for Nanoparticle Research, Institute for Basic Science (IBS), Seoul 08826, Korea; School of Chemical and Biological Engineering, Institute of Chemical Process Seoul National University, Seoul 08826, Korea; Institute of Engineering Research, College of Engineering, Seoul National University, Seoul 08826, Korea;* orcid.org/0000-0001-5959-6257

Complete contact information is available at: https://pubs.acs.org/10.1021/jacs.5c10868

Author Contributions

J.K., D.K., and S.S. equally contributed to this work.

Notes

The authors declare no competing financial interest.

■ ACKNOWLEDGMENTS

The authors gratefully acknowledge Professor John Straub and Professor Sangyoub Lee for their helpful comments. This work is supported by the Creative Research Initiative Project program (RS-2015-NR011925) and the Global Science Research Center Program (RS-2024-00411134) funded by the National Research Foundation of Korea, and the Samsung Electronics' University R&D program (IO240527-10099-01) (J.S.); National Research Foundation grant funded by the Korea government (MSIT) NRF-2020R1A2C1102788 (J.-H.K.); IBS-R006-D1 (T.H.); National Research Foundation grant funded by the Korea government (MSIT) NRF-2017R1A5A1015365, NRF-2020R1A2C2101871 (J.P.); National Research Foundation grant funded by the Korea government (MSIT) NRF-2021R1C1C1014339 (B.H.K.).

■ REFERENCES

(1) Murray, C.; Norris, D. J.; Bawendi, M. G. Synthesis and characterization of nearly monodisperse CdE (E= sulfur, selenium, tellurium) semiconductor nanocrystallites. *J. Am. Chem. Soc.* **1993**, *115* (19), 8706−8715.

(2) Alivisatos, A. P. Semiconductor clusters, nanocrystals, and quantum dots. *Science* **1996**, *271* (5251), 933−937.

(3) Brangwynne, C. P.; Eckmann, C. R.; Courson, D. S.; Rybarska, A.; Hoege, C.; Gharakhani, J.; Jülicher, F.; Hyman, A. A. Germline P granules are liquid droplets that localize by controlled dissolution/condensation. *Science* **2009**, *324* (5935), 1729−1732.

(4) Li, P.; Banjade, S.; Cheng, H.-C.; Kim, S.; Chen, B.; Guo, L.; Llaguno, M.; Hollingsworth, J. V.; King, D. S.; Banani, S. F. Phase transitions in the assembly of multivalent signalling proteins. *Nature* **2012**, *483* (7389), 336−340.

(5) Kok, J. F.; Adebiyi, A. A.; Albani, S.; Balkanski, Y.; Checa-Garcia, R.; Chin, M.; Colarco, P. R.; Hamilton, D. S.; Huang, Y.; Ito, A. Contribution of the world's main dust source regions to the global cycle of desert dust. *Atmos. Chem. Phys.* **2021**, *21* (10), 8169−8193.

(6) Adebiyi, A. A.; Kok, J. F. Climate models miss most of the coarse dust in the atmosphere. *Sci. Adv.* **2020**, *6* (15), No. eaaz9507.

(7) Marshall, J. S.; Palmer, W. M. K. THE DISTRIBUTION OF RAINDROPS WITH SIZE. *J. Atmos. Sci.* **1948**, *5* (4), 165−166.

(8) Niu, S.; Jia, X.; Sang, J.; Liu, X.; Lu, C.; Liu, Y. Distributions of raindrop sizes and fall velocities in a semiarid plateau climate: Convective versus stratiform rains. *J. Appl. Meteorol. Climatol.* **2010**, *49* (4), 632−645.

(9) Dusek, U.; Frank, G.; Hildebrandt, L.; Curtius, J.; Schneider, J.; Walter, S.; Chand, D.; Drewnick, F.; Hings, S.; Jung, D. Size matters more than chemistry for cloud-nucleating ability of aerosol particles. *Science* **2006**, *312* (5778), 1375−1378.
(10) Wood, R.; Field, P. R. The distribution of cloud horizontal sizes. *J. Clim.* **2011**, *24* (18), 4800−4816.
(11) Yang, F.; Kollias, P.; Shaw, R. A.; Vogelmann, A. M. Cloud droplet size distribution broadening during diffusional growth: ripening amplified by deactivation and reactivation. *Atmos. Chem. Phys.* **2018**, *18* (10), 7313−7328.
(12) Miles, N. L.; Verlinde, J.; Clothiaux, E. E. Cloud droplet size distributions in low-level stratiform clouds. *J. Atmos. Sci.* **2000**, *57* (2), 295−311.
(13) Schneider, R.; Maiolino, R. The formation and cosmic evolution of dust in the early Universe: I. Dust sources. *Astron. Astrophys. Rev.* **2024**, *32* (1), 2.
(14) Kroupa, P. The initial mass function of stars: evidence for uniformity in variable systems. *Science* **2002**, *295* (5552), 82−91.
(15) Ekimov, A. I. Quantum size effect in three-dimensional microscopic semiconductor crystals. *JETP Lett.* **1981**, *34*, 363.
(16) Rossetti, R.; Nakahara, S.; Brus, L. E. Quantum size effects in the redox potentials, resonance Raman spectra, and electronic spectra of CdS crystallites in aqueous solution. *J. Chem. Phys.* **1983**, *79* (2), 1086−1088.
(17) Litvin, A.; Martynenko, I.; Purcell-Milton, F.; Baranov, A.; Fedorov, A.; Gun'Ko, Y. Colloidal quantum dots for optoelectronics. *J. Mater. Chem. A* **2017**, *5* (26), 13252−13275.
(18) Yao, Y.-X.; Wan, J.; Liang, N.-Y.; Yan, C.; Wen, R.; Zhang, Q. Nucleation and growth mode of solid electrolyte interphase in Li-ion batteries. *J. Am. Chem. Soc.* **2023**, *145* (14), 8001−8006.
(19) Sneh, O.; Clark-Phelps, R. B.; Londergan, A. R.; Winkler, J.; Seidel, T. E. Thin film atomic layer deposition equipment for semiconductor processing. *Thin solid films* **2002**, *402* (1−2), 248−261.
(20) Wang, J.; Choi, J.-M.; Holehouse, A. S.; Lee, H. O.; Zhang, X.; Jahnel, M.; Maharana, S.; Lemaitre, R.; Pozniakovsky, A.; Drechsel, D. A molecular grammar governing the driving forces for phase separation of prion-like RNA binding proteins. *Cell* **2018**, *174* (3), 688−699. e616
(21) Brangwynne, C. P.; Tompa, P.; Pappu, R. V. Polymer physics of intracellular phase transitions. *Nat. Phys.* **2015**, *11* (11), 899−904.
(22) Choi, J.-M.; Hyman, A. A.; Pappu, R. V. Generalized models for bond percolation transitions of associative polymers. *Phys. Rev. E* **2020**, *102* (4), No. 042403.
(23) Gibbs, J. W. On the equilibrium of heterogeneous substances. *Am. J. Sci.* **1878**, *3*, 441−458.
(24) Frenkel, J. A general theory of heterophase fluctuations and pretransition phenomena. *J. Chem. Phys.* **1939**, *7* (7), 538−547.
(25) Frenkel, J. Statistical theory of condensation phenomena. *J. Chem. Phys.* **1939**, *7* (3), 200−201.
(26) Dillmann, A.; Meier, G. A refined droplet approach to the problem of homogeneous nucleation from the vapor phase. *J. Chem. Phys.* **1991**, *94* (5), 3872−3884.
(27) Hill, T. L.; Chamberlin, R. V. Extension of the thermodynamics of small systems to open metastable states: An example. *Proc. Natl. Acad. Sci. U. S. A.* **1998**, *95* (22), 12779−12782.
(28) Auer, S.; Frenkel, D. Prediction of absolute crystal-nucleation rate in hard-sphere colloids. *Nature* **2001**, *409* (6823), 1020−1023.
(29) Wolde, P. R. t.; Frenkel, D. Enhancement of protein crystal nucleation by critical density fluctuations. *Science* **1997**, *277* (5334), 1975−1978.
(30) Talapin, D. V.; Rogach, A. L.; Haase, M.; Weller, H. Evolution of an ensemble of nanoparticles in a colloidal solution: theoretical study. *J. Phys. Chem. B* **2001**, *105* (49), 12278−12285.
(31) Thanh, N. T.; Maclean, N.; Mahiddine, S. Mechanisms of nucleation and growth of nanoparticles in solution. *Chem. Rev.* **2014**, *114* (15), 7610−7630.
(32) Lutsko, J. F. How crystals form: A theory of nucleation pathways. *Sci. Adv.* **2019**, *5* (4), No. eaav7399.
(33) Emmerich, H.; Löwen, H.; Wittkowski, R.; Gruhn, T.; Tóth, G. I.; Tegze, G.; Gránásy, L. Phase-field-crystal models for condensed matter dynamics on atomic length and diffusive time scales: an overview. *Adv. Phys.* **2012**, *61* (6), 665−743.
(34) Lutsko, J. F. Density functional theory of inhomogeneous liquids. III. Liquid-vapor nucleation. *J. Chem. Phys.* **2008**, *129* (24), 244501.
(35) Oxtoby, D. W.; Evans, R. Nonclassical nucleation theory for the gas−liquid transition. *J. Chem. Phys.* **1988**, *89* (12), 7521−7530.
(36) Onuma, K.; Ito, A. Cluster growth model for hydroxyapatite. *Chem. Mater.* **1998**, *10* (11), 3346−3351.
(37) Gebauer, D.; Volkel, A.; Colfen, H. Stable prenucleation calcium carbonate clusters. *Science* **2008**, *322* (5909), 1819−1822.
(38) Baumgartner, J.; Dey, A.; Bomans, P. H.; Le Coadou, C.; Fratzl, P.; Sommerdijk, N. A.; Faivre, D. Nucleation and growth of magnetite from solution. *Nat. Mater.* **2013**, *12* (4), 310−314.
(39) Gebauer, D.; Kellermeier, M.; Gale, J. D.; Bergström, L.; Cölfen, H. Pre-nucleation clusters as solute precursors in crystallisation. *Chem. Soc. Rev.* **2014**, *43* (7), 2348−2371.
(40) Liu, M.; Wang, K.; Wang, L.; Han, S.; Fan, H.; Rowell, N.; Ripmeester, J. A.; Renoud, R.; Bian, F.; Zeng, J. Probing intermediates of the induction period prior to nucleation and growth of semiconductor quantum dots. *Nat. Commun.* **2017**, *8* (1), 15467.
(41) Wang, T.; Wang, Z.; Wang, S.; Chen, X.; Luan, C.; Yu, K. Thermally-Induced Isomerization of Prenucleation Clusters During the Prenucleation Stage of CdTe Quantum Dots. *Angew. Chem.* **2023**, *135* (43), No. e202310234.
(42) Williamson, M.; Tromp, R.; Vereecken, P.; Hull, R.; Ross, F. Dynamic microscopy of nanoscale cluster growth at the solid−liquid interface. *Nat. Mater.* **2003**, *2* (8), 532−536.
(43) Liao, H.-G.; Cui, L.; Whitelam, S.; Zheng, H. Real-time imaging of Pt_3Fe nanorod growth in solution. *Science* **2012**, *336* (6084), 1011−1014.
(44) Yuk, J. M.; Park, J.; Ercius, P.; Kim, K.; Hellebusch, D. J.; Crommie, M. F.; Lee, J. Y.; Zettl, A.; Alivisatos, A. P. High-resolution EM of colloidal nanocrystal growth using graphene liquid cells. *Science* **2012**, *336* (6077), 61−64.
(45) Jeon, S.; Heo, T.; Hwang, S.-Y.; Ciston, J.; Bustillo, K. C.; Reed, B. W.; Ham, J.; Kang, S.; Kim, S.; Lim, J. Reversible disorder-order transitions in atomic crystal nucleation. *Science* **2021**, *371* (6528), 498−503.
(46) Dachraoui, W.; Henninen, T. R.; Keller, D.; Erni, R. Multi-step atomic mechanism of platinum nanocrystals nucleation and growth revealed by in-situ liquid cell STEM. *Sci. Rep.* **2021**, *11* (1), 23965.
(47) Qiao, L.; Pollard, N.; Senanayake, R. D.; Yang, Z.; Kim, M.; Ali, A. S.; Hoang, M. T.; Yao, N.; Han, Y.; Hernandez, R. Atomically precise nanoclusters predominantly seed gold nanoparticle syntheses. *Nat. Commun.* **2023**, *14* (1), 4408.
(48) Kar, M.; Dar, F.; Welsh, T. J.; Vogel, L. T.; Kühnemuth, R.; Majumdar, A.; Krainer, G.; Franzmann, T. M.; Alberti, S.; Seidel, C. A. Phase-separating RNA-binding proteins form heterogeneous distributions of clusters in subsaturated solutions. *Proc. Natl. Acad. Sci. U. S. A.* **2022**, *119* (28), No. e2202222119.
(49) Gil-Garcia, M.; Benítez-Mateos, A. I.; Papp, M.; Stoffel, F.; Morelli, C.; Normak, K.; Makasewicz, K.; Faltova, L.; Paradisi, F.; Arosio, P. Local environment in biomolecular condensates modulates enzymatic activity across length scales. *Nat. Commun.* **2024**, *15* (1), 3322.
(50) Chakraborty, D.; Straub, J. E.; Thirumalai, D. Energy landscapes of Aβ monomers are sculpted in accordance with Ostwald's rule of stages. *Sci. Adv.* **2023**, *9* (12), No. eadd6921.
(51) Michaels, T. C.; Šarić, A.; Habchi, J.; Chia, S.; Meisl, G.; Vendruscolo, M.; Dobson, C. M.; Knowles, T. P. Chemical kinetics for bridging molecular mechanisms and macroscopic measurements of amyloid fibril formation. *Annu. Rev. Phys. Chem.* **2018**, *69* (1), 273−298.
(52) Hu, Q.; Nielsen, M. H.; Freeman, C.; Hamm, L.; Tao, J.; Lee, J.; Han, T. Y.-J.; Becker, U.; Harding, J.; Dove, P. The

thermodynamics of calcite nucleation at organic interfaces: Classical vs. non-classical pathways. *Faraday Discuss.* **2012**, *159* (1), 509−523.
(53) Habraken, W. J.; Tao, J.; Brylka, L. J.; Friedrich, H.; Bertinetti, L.; Schenk, A. S.; Verch, A.; Dmitrovic, V.; Bomans, P. H.; Frederik, P. M. Ion-association complexes unite classical and non-classical theories for the biomimetic nucleation of calcium phosphate. *Nat. Commun.* **2013**, *4* (1), 1507.
(54) Kim, J. H.; Yang, G. S.; Song, S.; Sung, J. Statistical Distribution of Laser-induced Growth of Nanoparticles: Effects of Laser Intensity and Medium−Nanoparticles Interactions. *Bull. Korean Chem. Soc.* **2015**, *36* (3), 914−918.
(55) Nelson, A.; Friedman, L. H. Thermodynamically stable colloidal solids: interfacial thermodynamics from the particle size distribution. *J. Phys. Chem. C* **2022**, *126* (4), 2161−2178.
(56) Kim, J.-H.; Kim, J.; Kim, B. H.; Song, S.; Kang, J.; Rhee, J.; Kim, D.; Chun, H.; Choi, H.; Cho, H. Multiphasic size-dependent growth dynamics of nanoparticle ensembles. *Proc. Natl. Acad. Sci. U. S. A.* **2025**, *122* (23), No. e2424950122.
(57) Singh, M. R.; Ramkrishna, D. Dispersions in crystal nucleation and growth rates: Implications of fluctuation in supersaturation. *Chem. Eng. Sci.* **2014**, *107*, 102−113.
(58) Chmiela, S.; Vassilev-Galindo, V.; Unke, O. T.; Kabylda, A.; Sauceda, H. E.; Tkatchenko, A.; Müller, K.-R. Accurate global machine learning force fields for molecules with hundreds of atoms. *Sci. Adv.* **2023**, *9* (2), No. eadf0873.
(59) Zeng, J.; Zhang, D.; Lu, D.; Mo, P.; Li, Z.; Chen, Y.; Rynik, M.; Huang, L. a.; Li, Z.; Shi, S. DeePMD-kit v2: A software package for deep potential models. *J. Chem. Phys.* **2023**, *159* (5), No. 054801.
(60) Batzner, S.; Musaelian, A.; Sun, L.; Geiger, M.; Mailoa, J. P.; Kornbluth, M.; Molinari, N.; Smidt, T. E.; Kozinsky, B. E (3)-equivariant graph neural networks for data-efficient and accurate interatomic potentials. *Nat. Commun.* **2022**, *13* (1), 2453.
(61) Lim, Y. R.; Park, S. J.; Song, S.; Yang, G.-S.; Yoon, Y.-G.; Kim, J.-H.; Sung, J. Exchange symmetry, fluctuation-compressibility relation, and thermodynamic potentials of quantum liquids. *Phys. Rev. E* **2014**, *89* (6), No. 062131.
(62) McClurg, R. B.; Flagan, R. C.; Goddard, W. A., III Free energy and surface tension of arbitrarily large Mackay icosahedral clusters. *J. Chem. Phys.* **1995**, *102* (8), 3322−3330.
(63) Sauceda, H. E.; Gálvez-González, L. E.; Chmiela, S.; Paz-Borbón, L. O.; Müller, K.-R.; Tkatchenko, A. BIGDML—Towards accurate quantum machine learning force fields for materials. *Nat. Commun.* **2022**, *13* (1), 3733.
(64) Han, S. S.; Kim, D.; Jung, D. H.; Cho, S.; Choi, S.-H.; Jung, Y. Accurate ab initio-based force field for predictive CO2 uptake simulations in MOFs and ZIFs: Development and applications for MTV-MOFs. *J. Phys. Chem. C* **2012**, *116* (38), 20254−20261.
(65) Yoshii, N.; Iwahashi, K.; Okazaki, S. A molecular dynamics study of free energy of micelle formation for sodium dodecyl sulfate in water and its size distribution. *J. Chem. Phys.* **2006**, *124* (18), 184901.
(66) Urano, R.; Pantelopulos, G. A.; Straub, J. E. Aerosol-OT surfactant forms stable reverse micelles in apolar solvent in the absence of water. *J. Phys. Chem. B* **2019**, *123* (11), 2546−2557.
(67) McClurg, R. B.; Flagan, R. C.; Goddard, W. A., III Thermodynamic properties and homogeneous nucleation rates for surface-melted physical clusters. *J. Chem. Phys.* **1996**, *105* (17), 7648−7663.
(68) Kim, D.; Choi, J. K.; Kim, S. M.; Hwang, I.; Koo, J.; Choi, S.; Cho, S. H.; Kim, K.; Lee, I. S. Confined nucleation and growth of PdO nanocrystals in a seed-free solution inside hollow nanoreactor. *ACS Appl. Mater. Interfaces* **2017**, *9* (35), 29992−30001.
(69) Kumar, A.; Jeon, K.-W.; Kumari, N.; Lee, I. S. Spatially confined formation and transformation of nanocrystals within nanometer-sized reaction media. *Acc. Chem. Res.* **2018**, *51* (11), 2867−2879.
(70) Oh, H. J.; Lee, Y.; Hwang, H.; Hong, K.; Choi, H.; Kang, J. Y.; Jung, Y. Size-controlled assembly of phase separated protein condensates with interfacial protein cages. *Nat. Commun.* **2025**, *16* (1), 1009.
(71) Yang, D. S.; Saeedi, A.; Davtyan, A.; Fathi, M.; Sherman, M. B.; Safari, M. S.; Klindziuk, A.; Barton, M. C.; Varadarajan, N.; Kolomeisky, A. B. Mesoscopic protein-rich clusters host the nucleation of mutant p53 amyloid fibrils. *Proc. Natl. Acad. Sci. U. S. A.* **2021**, *118* (10), No. e2015618118.
(72) Klass, S. H.; Gleason, J. M.; Omole, A. O.; Onoa, B.; Bustamante, C. J.; Francis, M. B. Preparation of Bioderived and Biodegradable Surfactants Based on an Intrinsically Disordered Protein Sequence. *Biomacromolecules* **2022**, *23* (3), 1462−1470.
(73) Tan, P.; Xu, N.; Xu, L. Visualizing kinetic pathways of homogeneous nucleation in colloidal crystallization. *Nat. Phys.* **2014**, *10* (1), 73−79.
(74) Deviri, D.; Pfeifer, C. R.; Dooling, L. J.; Ivanovska, I. L.; Discher, D. E.; Safran, S. A. Scaling laws indicate distinct nucleation mechanisms of holes in the nuclear lamina. *Nat. Phys.* **2019**, *15* (8), 823−829.
(75) Arai, S.; Tanaka, H. Surface-assisted single-crystal formation of charged colloids. *Nat. Phys.* **2017**, *13* (5), 503−509.
(76) Harris, J. J.; Pantelopulos, G. A.; Straub, J. E. Finite-size effects and optimal system sizes in simulations of surfactant micelle self-assembly. *J. Phys. Chem. B* **2021**, *125* (19), 5068−5077.
(77) Lee, O.-S.; Cho, V.; Schatz, G. C. Modeling the self-assembly of peptide amphiphiles into fibers using coarse-grained molecular dynamics. *Nano Lett.* **2012**, *12* (9), 4907−4913.
(78) Lee, J.; Baek, K.; Kim, M.; Yun, G.; Ko, Y. H.; Lee, N.-S.; Hwang, I.; Kim, J.; Natarajan, R.; Park, C. G. Hollow nanotubular toroidal polymer microrings. *Nat. Chem.* **2014**, *6* (2), 97−103.
(79) Luo, B.; Wang, Z.; Curk, T.; Watson, G.; Liu, C.; Kim, A.; Ou, Z.; Luijten, E.; Chen, Q. Unravelling crystal growth of nanoparticles. *Nat. Nanotechnol.* **2023**, *18* (6), 589−595.

https://doi.org/10.1021/jacs.5c10868
J. Am. Chem. Soc. 2025, 147, 46976−46985